JGR Oceans

RESEARCH ARTICLE
10.1029/2021JC017587

The Tropical Pacific Annual Cycle and ENSO in PMIP4 Simulations of the Mid-Holocene

Xiaolin Zhang[1,2], Alyssa R. Atwood[3], Bappaditya Nag[4,5], and Kim M. Cobb[6]

[1]Department of Earth and Planetary Sciences, Kyushu University, Fukuoka, Japan, [2]Oceanography Remote Sensing & Assimilation, University of Hamburg, Hamburg, Germany, [3]Department of Earth, Ocean, and Atmospheric Sciences, Florida State University, Tallahassee, FL, USA, [4]Geophysical Fluid Dynamics Institute, Florida State University, Tallahassee, FL, USA, [5]Indian Institute of Tropical Meteorology, Pune, India, [6]School of Earth and Atmospheric Sciences, Georgia Institute of Technology, Atlanta, GA, USA

Abstract We investigate the tropical Pacific annual cycle and the El Niño/Southern Oscillation (ENSO) in four mid-Holocene simulations. Our results show that both ENSO variability and the amplitude of the annual cycle of the tropical Pacific cold tongue are reduced under mid-Holocene forcing, along with a modified annual cycle in ENSO variance. The weakened annual cycle of the cold tongue is attributed to an ocean dynamical response to westerly wind anomalies in the western equatorial Pacific in boreal spring in addition to a thermodynamic response to local insolation changes in the eastern Pacific. The anomalous westerly winds in boreal spring excite an annual downwelling Kelvin wave that deepens the thermocline and propagates eastward along the equator, reaching the central and eastern equatorial Pacific during the development season of ENSO in boreal summer. Upon reaching the eastern Pacific, the downwelling Kelvin wave deepens the near-surface thermocline, warming the surface ocean and weakening the local ocean-atmosphere coupling critical to the growth of ENSO events. The westerly wind anomaly is associated with a shift in convection in the western Pacific driven by greater cooling of the Maritime Continent than western Pacific Ocean during the first half of the year (January to June) under tropical insolation forcing. By elucidating a common set of mechanisms responsible for a reduced cold tongue annual cycle and ENSO variability in a diverse range of mid-Holocene simulations, this work yields important insight into the linkages between the tropical Pacific annual cycle and ENSO that are critical for understanding tropical Pacific climate variability.

Plain Language Summary Paleoclimate records and climate models alike indicate that the tropical Pacific underwent substantial changes during the mid-Holocene, including weakened variability associated with the El Niño/Southern Oscillation (ENSO). In this study, we analyzed four global climate models included in the latest Paleoclimate Model Intercomparison Project and show that seasonal changes in the amount of sunlight received by the tropics caused a weakened annual cycle of sea surface temperatures in the eastern Pacific Ocean due in part to changes in wind and rainfall patterns in the western Pacific. These changes in the annual cycle cause ENSO variability to be reduced because the coupling between the ocean and atmosphere is weakened during the part of the year that is important for the growth of ENSO events. These findings support previous results that highlight an important linkage between changes in the tropical Pacific annual cycle and ENSO during the mid-Holocene.

Key Points:

- The annual cycle of the tropical Pacific cold tongue and El Niño/Southern Oscillation (ENSO) variability is reduced during the mid-Holocene in PMIP4 models
- Westerly wind anomalies in the western Pacific in boreal spring drive an annual downwelling Kelvin wave that deepens the eastern equatorial Pacific thermocline in boreal summer
- The westerly wind anomaly is associated with a shift in convection driven by differential cooling of the Maritime Continent and western Pacific in response to insolation forcing

Supporting Information:

Supporting Information may be found in the online version of this article.

Correspondence to:

X. Zhang,
zhang.xiaolin.277@m.kyushu-u.ac.jp

Citation:

Zhang, X., Atwood, A. R., Nag, B., & Cobb, K. M. (2022). The tropical Pacific annual cycle and ENSO in PMIP4 simulations of the mid-Holocene. *Journal of Geophysical Research: Oceans*, *127*, e2021JC017587. https://doi.org/10.1029/2021JC017587

Received 18 MAY 2021
Accepted 25 JUL 2022
Corrected 21 SEP 2022

This article was corrected on 21 SEP 2022. See the end of the full text for details.

Author Contributions:

Conceptualization: Xiaolin Zhang, Alyssa R. Atwood, Bappaditya Nag, Kim M. Cobb
Methodology: Bappaditya Nag
Supervision: Alyssa R. Atwood, Kim M. Cobb
Writing – original draft: Xiaolin Zhang
Writing – review & editing: Alyssa R. Atwood, Bappaditya Nag, Kim M. Cobb

1. Introduction

The El Niño/Southern Oscillation (ENSO) is the most pronounced interannual climate phenomenon on a global scale and it has major impacts on the natural environment and human societies around the world. ENSO is tightly coupled to the mean state of the tropical Pacific and its annual cycle (e.g., Battisti & Hirst, 1989; Zebiak & Cane, 1987). For example, the seasonal variation of tropical Pacific climate plays a key role in the onset and termination of ENSO events. The variation in the annual cycle of the tropical Pacific cold tongue can modulate the strength of the Bjerknes feedback—the positive feedback loop responsible for the growth of ENSO events (Jin et al., 1994, 1996; Tziperman et al., 1994, 1995; Wang & Fang, 1996). The seasonal migration of the South Pacific Convergence Zone (SPCZ) also plays a key role in ENSO modulation, via the termination of strong El Niño events (Harrison & Vecchi, 1999; McGregor et al., 2012; Stein et al., 2011). However, the coupling between the annual cycle of the tropical Pacific and ENSO variability is not fully understood, particularly on long time scales.

The Holocene epoch serves as a valuable target to investigate the dynamics of ENSO and assess its sensitivity to external forcing. Paleoclimate records from the tropical Pacific indicate that ENSO variability was reduced by as much as 50%–80% from 3,000 to 6,000 years before the present (i.e., the mid-to-late Holocene), a time when Earth's orbital parameters were substantially different than those of today (Carré et al., 2021; Cobb et al., 2013; Emile-Geay et al., 2016; Koutavas & Joanides, 2012; McGregor et al., 2013).

Several mechanisms have been proposed to explain the reduction of ENSO variability during this period. Numerous modeling studies have demonstrated that orbital forcing modulates the strength of ENSO feedbacks in the tropical Pacific, limiting the development of large ENSO events (Clement et al., 1999; Karaperidou et al., 2015; Liu et al., 2014; Roberts et al., 2007). However, the mechanisms by which insolation changes modulate ENSO feedbacks vary widely across models. Other studies have proposed that the Holocene ENSO minimum was caused by enhanced seasonality in the tropical Pacific through the nonlinear mechanism of frequency entrainment (Pan et al., 2005). More specifically, when a strong equatorial annual cycle forcing is present, the amplitude of ENSO events tends to be reduced due to its interaction with the annual cycle (Chang et al., 1994; Liu, 2002). However, paleoclimate reconstructions indicate that seasonality in the central and eastern tropical Pacific was actually reduced during most of the mid-to-late Holocene (Carré et al., 2021). Other proposed mechanisms of the Holocene ENSO minimum include drivers that operate outside the tropical Pacific, including the advection of subsurface temperature anomalies from the extratropical ocean (Liu et al., 2000) and reduced extratropical atmospheric forcing (Chiang et al., 2009).

Model intercomparison studies have found that ENSO variability was modestly reduced in multiple generations (PMIP2, PMIP3, and PMIP4) of mid-Holocene simulations (An & Choi, 2014; Brown et al., 2020; Emile-Geay et al., 2016; Song & Chen, 2022). Karamperidou et al. (2015) demonstrated a plausible link between reduced ENSO variability and the tropical Pacific annual cycle in the Community Climate System Model version 4 (CCSM4), whereby the variance of eastern Pacific El Niño events was reduced by 30% in the mid-Holocene due to seasonal wind forcing in the western Pacific. They demonstrated that weakened trade winds in the western equatorial Pacific in early boreal spring initiated an anomalous downwelling Kelvin wave that propagated eastward to the eastern Pacific during the ENSO development season in boreal summer and fall, reducing the upper ocean stratification and thereby reducing the ENSO upwelling feedback. Alongside a reduction in eastern Pacific ENSO variability, these same processes also drove a weakened annual cycle of sea surface temperatures (SSTs) in the tropical Pacific cold tongue (Karamperidou et al., 2015). Similar changes in the tropical Pacific annual cycle under mid-Holocene forcing have also been found in PMIP3 intermodel comparison studies (Emile-Geay et al., 2016; Erb et al., 2015). In the PMIP3 mid-Holocene simulations, the amplitude of the tropical Pacific annual cycle is reduced by 10%–50% across models (Emile-Geay et al., 2016). Given the demonstrated linkages between the tropical Pacific annual cycle and ENSO in today's climate, such changes in the tropical Pacific annual cycle are expected to have important implications for ENSO during the mid-Holocene.

We investigate the tropical Pacific annual cycle and ENSO in four mid-Holocene simulations included in the Paleoclimate Modeling Intercomparison Project—Phase 4 (PMIP4). These models are: the National Center for Atmospheric Research Community Earth System Model version 2 (CESM2), the Japan Meteorological Agency Meteorological Research Institute Earth System Model Version 2.0 (MRI-ESM2.0), the Model for Interdisciplinary Research on Climate, Earth System version 2 for Long-term simulations (MIROC-ES2L) and the National Aeronautics and Space Administration Goddard Institute for Space Studies model (GISS-E2-1-G). A brief description of the models is provided in Section 2. Sections 3.1 and 3.2 describe the simulated changes in ENSO and the tropical Pacific annual cycle between the mid-Holocene and pre-industrial simulations. Section 3.3 discusses possible mechanisms responsible for these changes. Concluding remarks and further discussion are provided in Section 4.

2. Methods

CESM2 is a coupled climate/Earth system model (Danabasoglu et al., 2019). The horizontal resolution of the preindustrial control simulation is nominal 1° in the atmosphere and the ocean. The atmosphere has 32 vertical levels up to 2.26 hPa and the ocean has 60 vertical levels. MRI-ESM2.0 has a horizontal resolution of 100 km in the atmosphere and ocean, and the atmospheric vertical resolution is 80 layers (Yukimoto et al., 2019).

MIROC-ES2L has a horizontal resolution in the atmosphere of approximately 2.8° latitude and longitude (T42 spectral truncation) and the vertical resolution is 40 levels up to 3 hPa (Hajima et al., 2020). The horizontal resolution of the ocean is nominal 1° and the vertical resolution of the ocean is 62 layers. GISS-E2-1-G (Kelley et al., 2020) has a horizontal resolution of 2° latitude by 2.5° longitude in the atmosphere and nominal 1° latitude by 1.25° longitude in the ocean.

The experimental design for the PMIP4 mid-Holocene experiments is described in Otto-Bliesner et al. (2017). Atmospheric greenhouse gas concentrations and orbital parameters follow the PMIP4 mid-Holocene experiment procedures (Otto-Bliesner et al., 2017). Namely, CO_2 = 264.4 ppm, CH_4 = 597 ppb, and N_2O = 262 ppb, eccentricity is 0.018682, the obliquity is 24.105° and the longitude of perihelion is 0.87° (compared to 100.33° in the control run). The last 100 years of the mid-Holocene simulations were analyzed in this study.

The dominant forcing mechanism of the mid-Holocene is insolation forcing associated with changes in the precessional cycle, which produces insolation anomalies of up to ±20 W/m^2 that vary as a function of month and latitude. These substantial changes in the latitudinal and seasonal distribution of solar insolation can cause large changes in tropical climate (Karaperidou et al., 2015; Schneider et al., 2014). During the mid-Holocene, equatorial insolation increases in boreal summer and fall (May to October) and decreases in boreal winter and spring (November to April; Figure S2 in Supporting Information S1). The insolation changes in the tropics lag those in the extratropical Northern Hemisphere by approximately a month.

To compare ENSO characteristics in the models with observational data, monthly mean SSTs from the NOAA Extended Reconstructed Sea Surface Temperature (ERSST) version 5 were analyzed. This data set spans the period from January 1970 to December 2019 and has a spatial resolution of 2° latitude × 2° longitude. The amplitude of the SST annual cycle in the Niño3 and Niño3.4 regions was quantified as the range (maximum − minimum) of the monthly mean seasonal cycle in SST (i.e., the SST climatology for each calendar month). The Niño3 and Niño3.4 SST anomalies (SSTAs) from the annual cycle were calculated by removing the monthly climatology from the monthly SSTs. The Niño3.4 region is defined by the box bounded by 5°S–5°N, 170°W–120°W and Niño3 region is defined by the box bounded by 5°S–5°N, 150°W–90°W.

3. Results and Discussion

3.1. Characteristics of ENSO and the Tropical Pacific Annual Cycle in Control Simulations Versus Observations

3.1.1. Spatial Pattern and Variance of ENSO

ENSO emerges as the first EOF of observed monthly SST anomalies in the equatorial Pacific Ocean (15°S–15°N, 140°E–90°W), accounting for 73% of the variance in ERSSTv5 (Figure 2a). The simulated ENSO pattern in the preindustrial control run of each of the four models (MIROC, MRI, CESM, and GISS) is broadly similar to observations, aside from the well-known model bias of ENSO events extending farther westward than observations (Figure 2). The ENSO pattern explains 75% of the variance in MIROC, 73% in MRI, 77% in CESM and 86% in GISS. The control runs of MRI and MIROC exhibit ENSO variability that is similar to observations, while the control runs of GISS and CESM exhibit ENSO variability that is substantially higher than observed (Figures 2 and 3).

3.1.2. Phase Locking of ENSO to the Calendar Year

As described in Clarke and Zhang (2019), a fundamental feature of ENSO and its prediction is the phase locking of ENSO events to the calendar year. Specifically, to within an excellent approximation (see Figure 2 in Clarke and Zhang (2019)), the Niño3.4 index can be written as a fixed calendar month structure beginning in April of one calendar year and ending in March of the following year, and a single annual value for a particular El Niño/La Niña year that begins in April of 1 year and end in March of the following year ($Y(a)$). For example, the big El Niño year from April 1997 to March 1998 corresponds to a large positive $Y(a)$, while the big La Niña from April 1988 to March 1989 corresponds to a large negative value of $Y(a)$ and both have the same phase-locked structure. The phase-locked structure indicates that El Niño and La Niña events tend to maximize near the end of the calendar year and that they all can be well approximated by a single annual function $Y(a)$ multiplied by a fixed

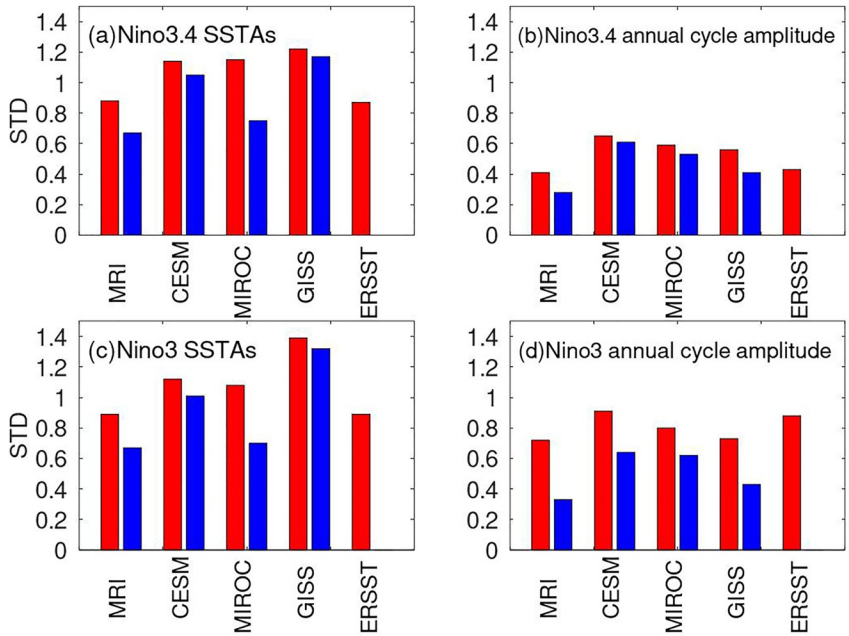

Figure 1. (a) Standard deviation of Niño3.4 sea surface temperature (SST) anomalies and (b) the annual cycle amplitude (see Section 2) in the Niño3.4 region for piControl runs (red bar) and mid-Holocene runs (blue bar) in each model. (c–d) are the same as (a–b), but for the Niño3 region. The last red bar indicates observational data from ERSST-V5 for the period 1970 to 2019.

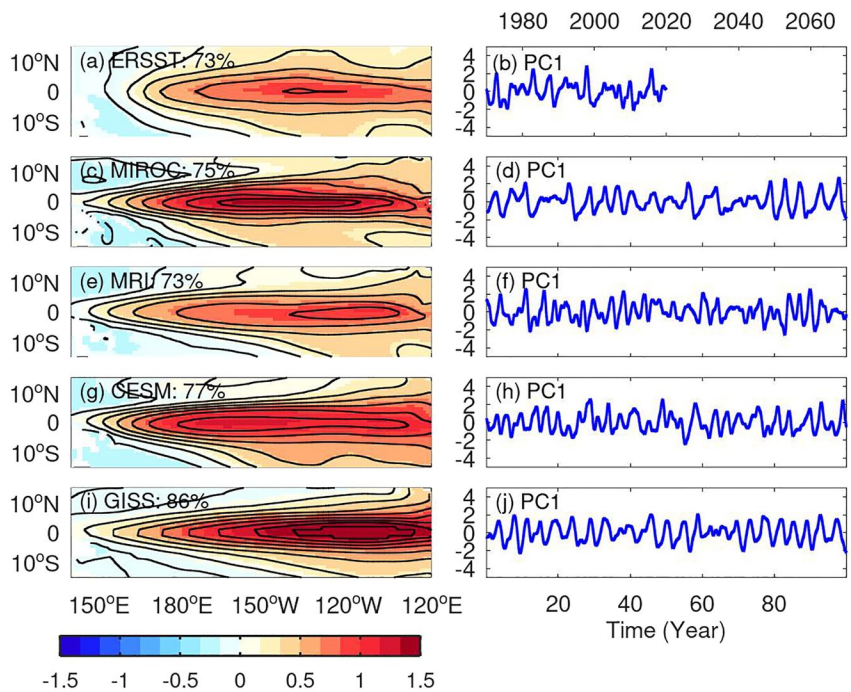

Figure 2. The first Empirical Function (EOF1) spatial pattern for (a) ERSST, (c) MIROC, (e) MRI, (g) CESM and (i) GISS model. (b, d, f, h, and j) are the corresponding first principal component (unit: °C). The values listed in the left-hand panels indicate the percentage of sea surface temperature (SST) variance explained by EOF1.

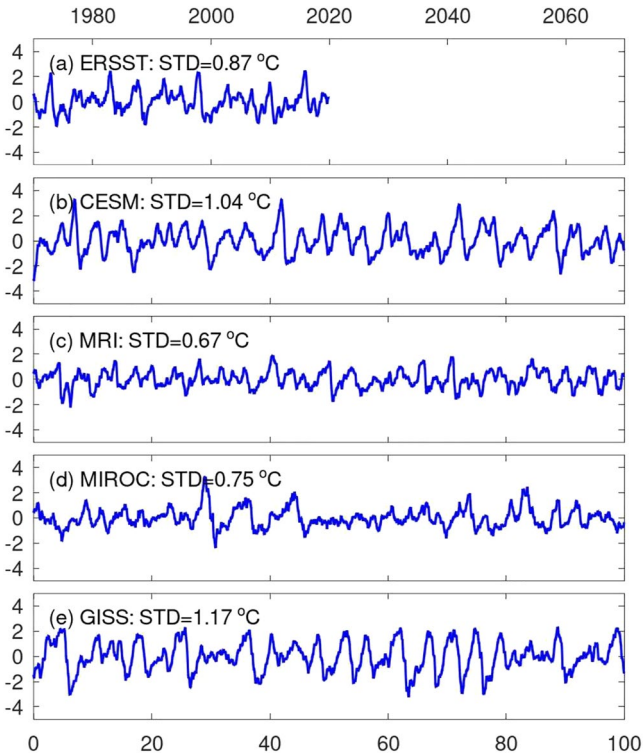

Figure 3. Time series of monthly SST anomalies in the Niño3.4 region (unit: °C) from (a) observations (ERSSTV5), (b) CESM, (c) MRI, (d) MIROC and (e) GISS piControl runs. The standard deviation of each time series is listed in each panel.

structure function $S(m)$. The spring persistence barrier, first documented by Walker (1924), and now often studied (see, e.g., the review by Clarke, 2014), is closely associated with the phase-locked structure and the uncertainty in what Y in year $a + 1$ will be given Y in year a.

The observed annual cycle of variance in the Niño3.4 index is shown in Figure 5. ENSO variance is highest in January (1.3°C) and lowest in April to June (0.8°C). In the control simulations, the annual cycle in variance differs greatly across models: GISS and MIROC demonstrate very weak phase locking (particularly in GISS, which exhibits no clear annual cycle in variance; Figure 5). CESM and MRI exhibit a more realistic phase locking structure and amplitude, although in both models, the month of minimum variance is offset by approximately 2 months (i.e., the variance minimizes in June/July instead of the observed April/May).

3.1.3. Tropical Pacific Annual Cycle

The observed annual cycle of equatorial Pacific SSTs is characterized by strong seasonal variation in the eastern Pacific cold tongue, with the coldest temperatures attained from August through November (reaching as low as 24°C). SSTs increase westward, forming the Western Pacific Warm Pool with maximum SSTs above 28°C that extend eastward from January to April (reaching as far east as 170°W) and retreat westward from May to July. The observed annual cycle of tropical Pacific SSTs is simulated relatively well in the preindustrial control simulations (Figure 4). The simulations exhibit strong seasonal variation in the eastern equatorial Pacific with maximum SSTs in boreal spring and minimum SSTs in boreal summer and fall. SSTs in the western equatorial Pacific are several degrees warmer than SSTs in the east and exhibit substantially less seasonal variation. Modest biases in the annual cycle do exist in the simulations and vary across models. For example, GISS exhibits an early termination to the coldest phase of the cold tongue while CESM and MRI exhibit a cold bias during the warm phase of the cold tongue (Figure 4).

The mean annual SST biases in the tropical Pacific (i.e., the difference between the control run and observations) is shown for each model in Figure S1 in Supporting Information S1. The models exhibit a wide range of SST biases, including a cool bias in the northern tropical Pacific around 20°–30°N that is most pronounced in MIROC and a strong warm bias off the coast of South America (associated with low-cloud biases) that approaches 5°C in GISS. All models also exhibit positive SST biases adjacent to the Baja California Peninsula and negative SST biases downwind of the southern Sierra Madre mountain range, where orographic biases insufficiently block the flow of the tropical easterly trade winds and lead to low-level wind biases in the eastern Pacific (Baldwin et al., 2021). The equatorial Pacific is characterized by a negative SST bias reaching 1°C in MRI, MIROC, and CESM.

3.2. Simulated Changes in Tropical Pacific Climate During the Mid-Holocene

3.2.1. Changes in the Annual Cycle of Equatorial Pacific SSTs During the Mid-Holocene

In response to precessional forcing during the mid-Holocene, the cold tongue is warmed from July to December (~0.5°C), when the cold tongue is most developed and it is cooled from January to June (~1°C), when the cold tongue is less developed (Figure 4). These changes counteract the climatological annual cycle and thus dampen the amplitude of the tropical Pacific annual cycle in the models. The amplitude of the SST annual cycle in the Niño3.4 region is reduced by 32% in MRI, 6% in CESM, 10% in MIROC and 25% in GISS. In addition to the changes in the annual cycle, annual mean SSTs are also modified during the mid-Holocene. Namely, mean SSTs decrease across large parts of the tropical Pacific by up to −1.0°C in MRI, 0.7°C in CESM, 1.1°C in MIROC and 0.6°C in GISS, with a spatial pattern that varies widely across models (Figure 6).

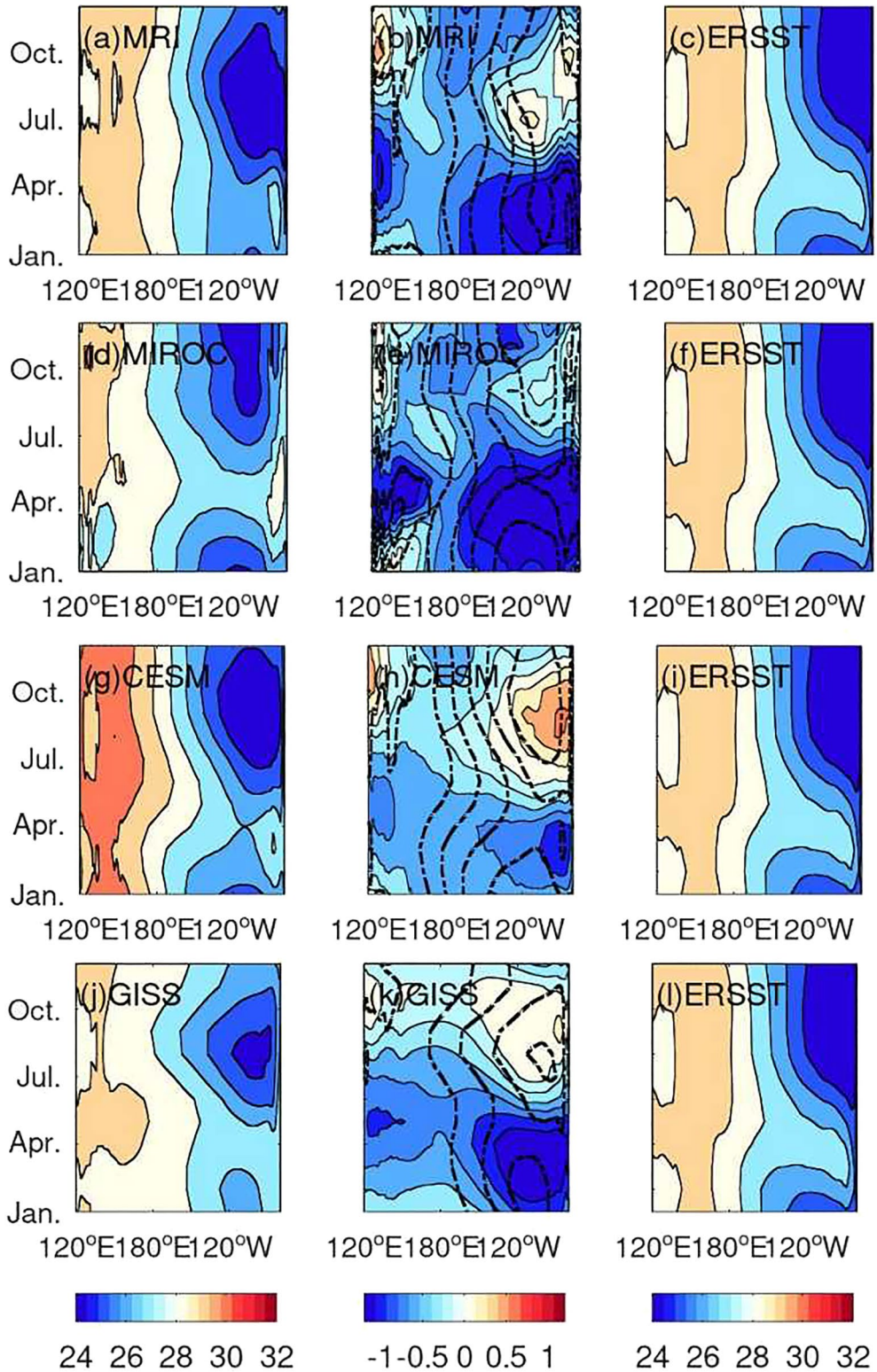

Figure 4. Monthly climatology of equatorial (5°S–5°N) Pacific SSTs and SST differences for each model (MRI: first row, MIROC: second row, CESM: third row and GISS: fourth row). The colored contours in the first column indicate SSTs in the piControl run. In the second column, the colored contours indicate the difference between the mid-Holocene runs and the piControl runs (mid-Holocene—piControl) and the dashed contours indicate SSTs in the mid-Holocene run. In the third column, the colored contours indicate SSTs in observational data (ERSSTV5).

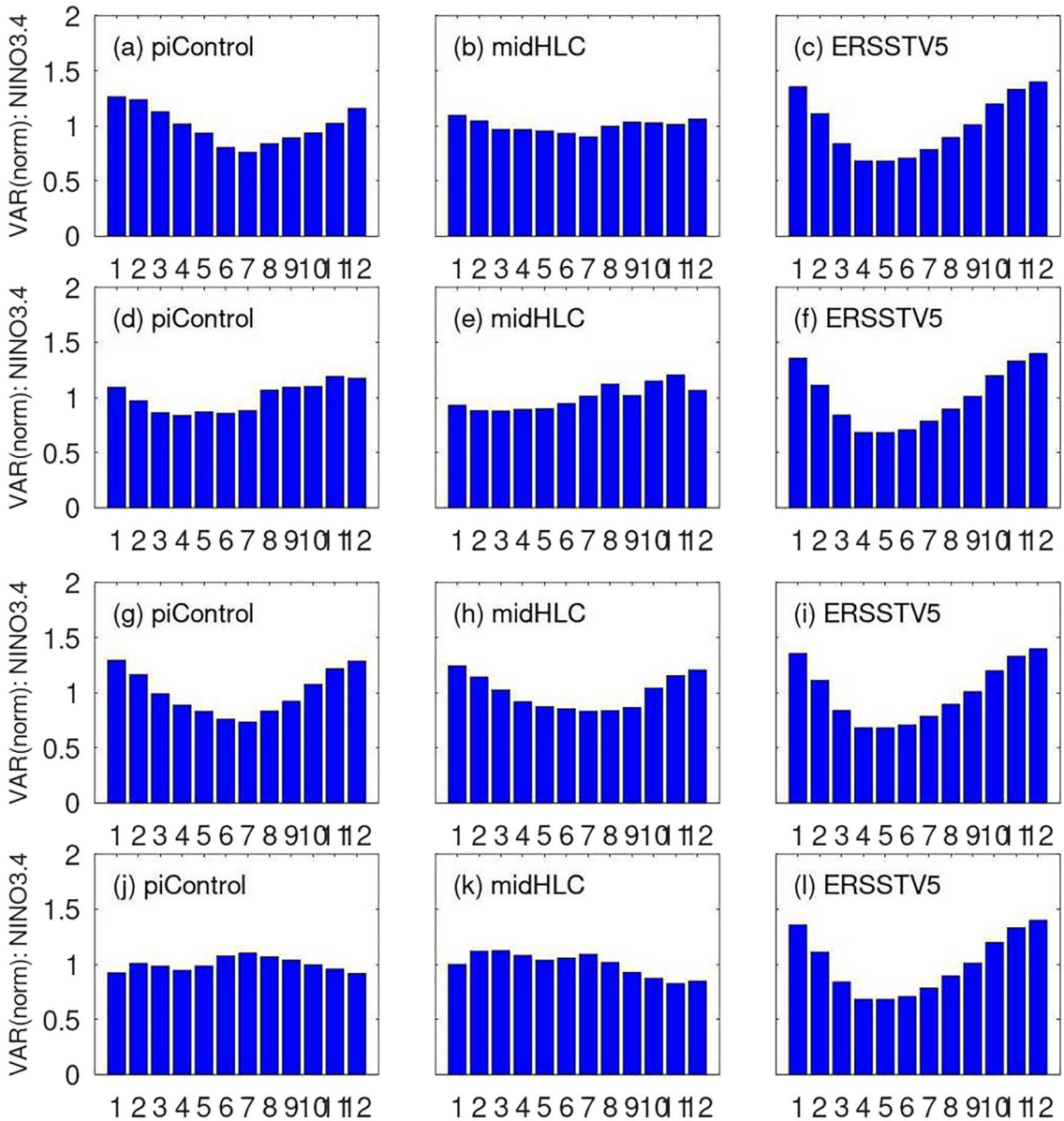

Figure 5. Variance of Niño3.4 sea surface temperature (SST) anomalies in the piControl and mid-Holocene runs of (a-b) MRI, (d-e) MIROC, (g-h) CESM and (j-k) GISS model. The variance has been normalized by the long-term variance (so that the average variance across the 12 months of the year is equal to 1). Observational data from ERSSTV5 are plotted in the last column.

3.2.2. Changes in ENSO During the Mid-Holocene

During the mid-Holocene, ENSO variability in the Niño3 and Niño3.4 regions is reduced in all models (Figure 1). The standard deviation of Niño3.4 SSTAs is reduced by 24% in MRI, 8% in CESM, 34% in MIROC and 4% in GISS. The fact that ENSO variability is reduced alongside a reduction in the annual cycle of the cold tongue indicates that the frequency entrainment mechanism is not supported in these models. In addition to the overall reduction in ENSO variability, the phase locking of ENSO to the calendar year is also modified (Figure 5). In three out of the four models (CESM, MRI, and MIROC), ENSO is more weakly phase locked to the calendar year, while in GISS the phase locking remains weak, but the timing of maximum and minimum variance has shifted.

We conclude that the tropical Pacific annual cycle and ENSO variability is weakened in each of the four CMIP6 models in response to precessional forcing during the mid-Holocene. The phase locking of ENSO to the annual cycle is also weakened in three out of the four models. In the following sections, we explore the

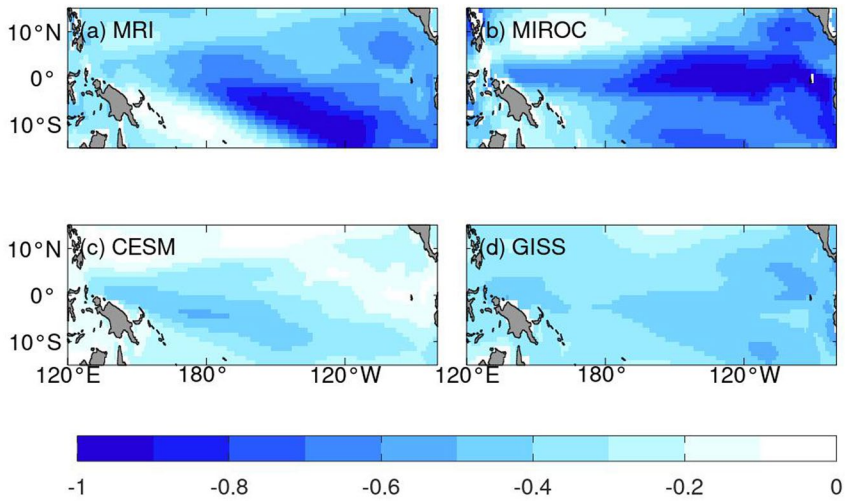

Figure 6. Change in mean annual sea surface temperature (unit: °C) in each model (mid-Holocene—piControl).

possible dynamics responsible for the simulated reduction in the cold tongue annual cycle and ENSO variability.

3.3. Mechanisms of a Reduced Cold Tongue Annual Cycle and ENSO Variability During the Mid-Holocene

Several different mechanisms have been proposed as the driver of reduced ENSO variability during the mid-Holocene. The nonlinear mechanism of frequency entrainment is one such mechanism (e.g., Chang et al., 1994; Jin et al., 1994; Liu, 2002; Tziperman et al., 1994). However, since both the annual cycle and ENSO variability are reduced in the PMIP4 simulations, the frequency entrainment mechanism is not supported by these models. Other mechanisms involve various ways in which orbital forcing modulates the strength of ocean–atmosphere feedbacks in the tropical Pacific Ocean that are critical to the growth of ENSO events (Karaperidou et al., 2015; Liu et al., 2014). In the following section, we investigate a set of mechanisms by which orbital forcing drives changes in both the tropical Pacific annual cycle and ENSO in detail.

3.3.1. Dynamical Response of the Equatorial Pacific Ocean to Western Pacific Wind Stress Changes

From January to February, a pronounced westerly wind stress anomaly develops in the western equatorial Pacific in all models (Figure 7i–7l). This westerly wind stress anomaly originates around 120°E−140°E and propagates eastward from February to May, eventually extending beyond the dateline. In association with this westerly wind stress anomaly, the depth of the thermocline along the equator (as represented by the 20° isotherm) increases by up to 10–15 m in the western Pacific Ocean and propagates eastward as a Kelvin wave beginning in January/February, reaching the eastern equatorial Pacific in June/July (Figures 7a–7d). Importantly, this results in a deepening of the central and eastern Pacific thermocline during boreal summer, which is a critical period of growth for ENSO events. As the thermocline anomaly travels eastward, it rises to the surface following the climatological thermocline, eventually warming the surface and reducing the upper ocean stratification upon reaching the central and eastern Pacific in June/July (Figures 7e–7h). Karamperidou et al. (2015) demonstrated that in CCSM4 these conditions act to reduce the upwelling feedback during the ENSO development season and drive reduced variance of eastern Pacific El Niño events and a 2-month delay in their peak month (from December to February).

A corresponding positive SST anomaly develops in the central equatorial Pacific around June/July, propagating eastward to the far eastern Pacific and peaking between August to October (Figures 7e–7h). The peak SST anomaly lags the peak thermocline anomaly in the eastern Pacific by 1–3 months. This lag reflects the fact that there is an additional contribution to the warming tendency in the eastern equatorial Pacific surface ocean that is slightly offset in time relative to the thermocline depth anomaly just described (which warms the central/eastern Pacific in June/July). The source of the additional warming is the increased equatorial insolation from May to October under precessional forcing (Figure S2 in Supporting Information S1). This implies that the warming of the Pacific cold tongue in boreal summer and fall is driven by both dynamical and thermodynamical components. The zonal wind stress, thermocline depth, and SST responses just described are generally consistent across models, albeit with differing magnitudes-the wind stress and thermocline depth anomalies are largest in MIROC and MRI and weakest in CESM and GISS (Figure 7).

In summary, these dynamic and thermodynamic components of the cold tongue response drive a warming tendency in the cold tongue from July to December, when the cold tongue is most developed and a cooling tendency from January to June, when the cold tongue is least developed (Figure 5). Because these changes counteract the climatological annual cycle, they dampen the annual cycle of the tropical Pacific cold tongue in the models. If, as we have speculated, the deepening of the central and eastern Pacific thermocline during the ENSO growth season in boreal summer is indeed tied to the weakened ENSO variability in the mid-Holocene simulations, this would demonstrate a mechanistic link between orbital forcing and simultaneous reductions

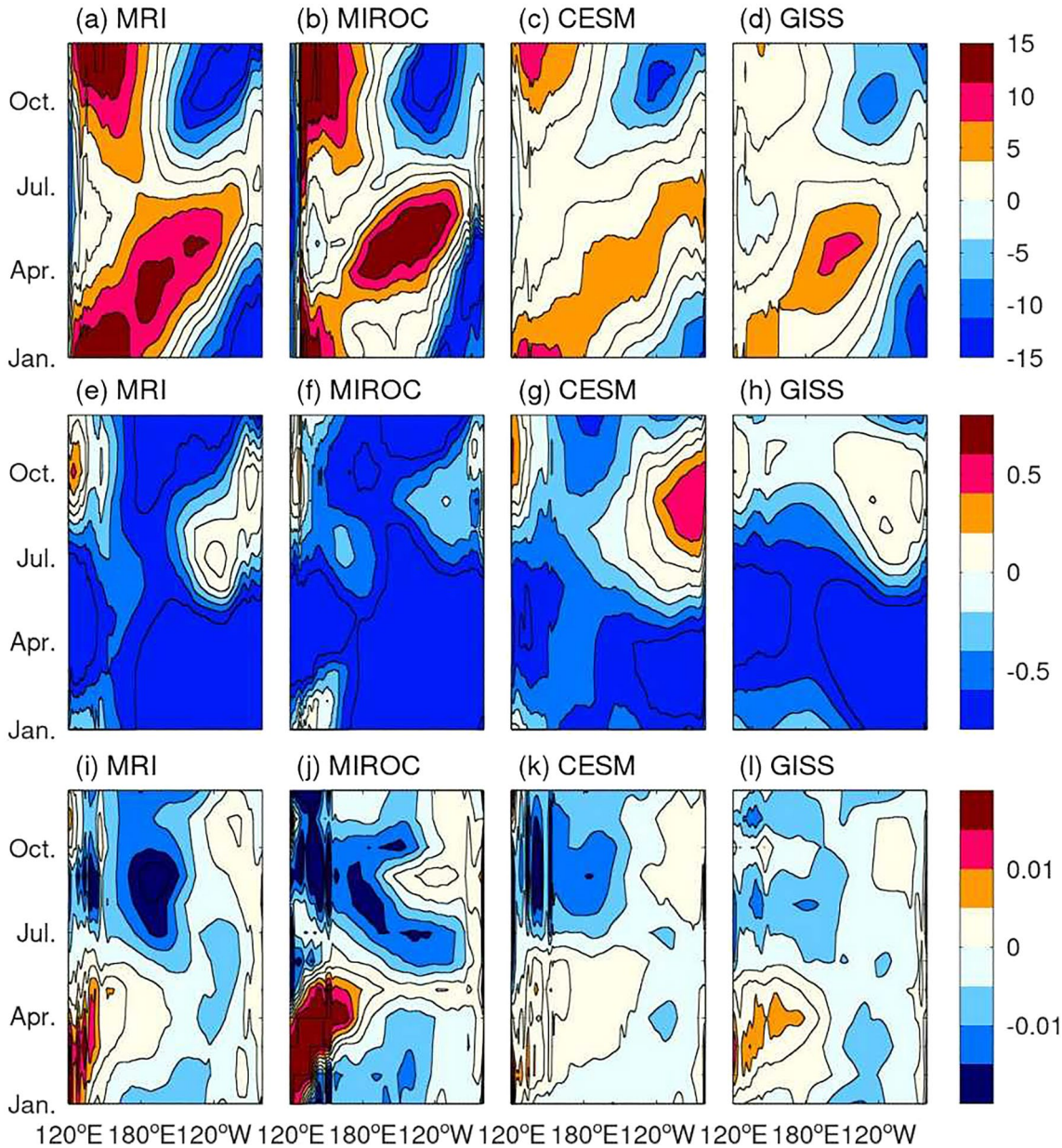

Figure 7. Change in monthly climatology in each model of: (a–d) equatorial 20°C isotherm depth (unit: m), (e–h) equatorial sea surface temperatures (SSTs) (unit: °C), (i–l) zonal windstress (unit: dyn/cm^2). In each panel, the differences are taken as mid-Holocene minus piControl, and the data are averaged over 5°S–5°N.

in the tropical Pacific annual cycle and ENSO variability, driven by dynamical ocean adjustment during the mid-Holocene.

In the following sections, we investigate the mechanisms of the westerly wind stress anomalies that are responsible for this dynamical ocean adjustment.

3.3.2. Thermally-Driven Shift in Convection and Winds Over the Western Equatorial Pacific

Previous studies have suggested that shifts in convection over the Maritime Continent are responsible for the westerly wind stress anomaly in the western Pacific Ocean during the mid-Holocene (Erb et al., 2015). Rainfall over the Maritime Continent is driven by a complex set of interactions between the South Asian summer monsoon

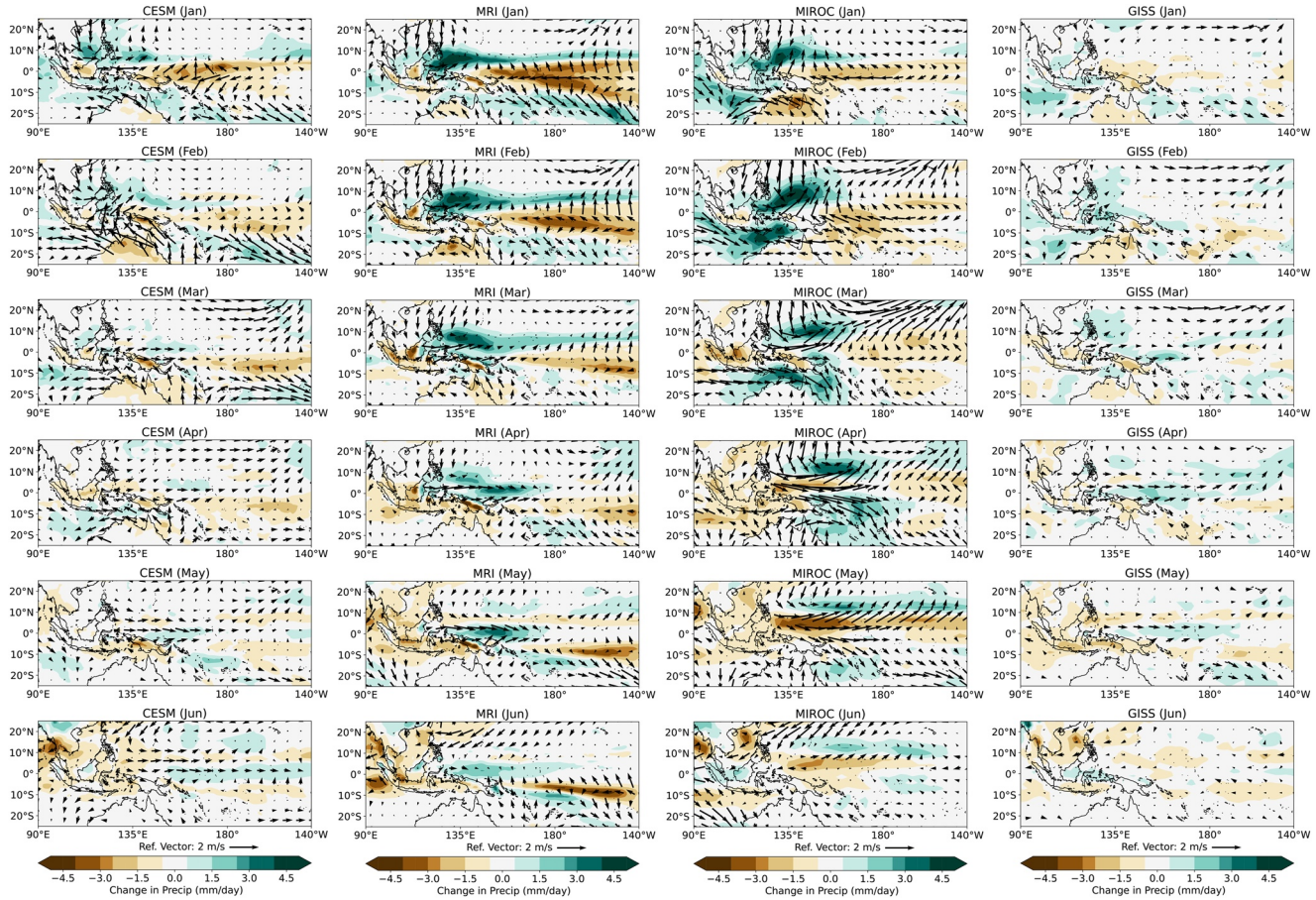

Figure 8. Change in precipitation (color shading; units mm/day) and near surface winds (vectors) for each model (mid-Holocene minus piControl).

and the Australian summer monsoon, in tandem with the local orography (Chang et al., 2005). These monsoonal circulations drives a strong annual cycle and a weaker semiannual cycle in rainfall over the Maritime Continent.

During the mid-Holocene, widespread cooling occurs from January through April across the entire western boundary of the Pacific, from Asia, across the Maritime Continent, to Australia (Figure 10) following global reductions in insolation (Figure S2 in Supporting Information S1). Initially, in January/February, this cooling is associated with a negative sea level pressure anomaly between Southeast Asia and the northern extent of the Maritime Continent, which drives a cyclonic circulation anomaly in the low-level winds. This circulation anomaly is the source of the initiation of the westerly wind anomalies in the western equatorial Pacific, which extend along and to the north of the equator. From March to June, the westerly wind anomalies strengthen and become more zonally oriented along the equator, even as the cyclonic circulation feature disappears, due to the local SST gradient develops between the Maritime Continent and the western Pacific. The differing thermal properties of the Maritime Continent and western Pacific Ocean likely lead to this land-ocean heating contrast whereby the Maritime Continent cools more than the Western Pacific ocean in response to reduced tropical insolation. The tropical land cooling is most pronounced in March and April, when the westerly wind anomalies also tend to maximize (Figure 10).

The resulting zonal temperature gradient drives a shift in convection from land to ocean regions in the Maritime Continent and the western Pacific, as demonstrated by precipitation anomalies in this region from January to May (Figure 8). While substantial differences exist across models in the low-level circulation and precipitation responses, all models tend to show reduced precipitation over land and increased precipitation over ocean regions, including the western equatorial Pacific, particularly from March to May (Figure 8). This shift in convection is

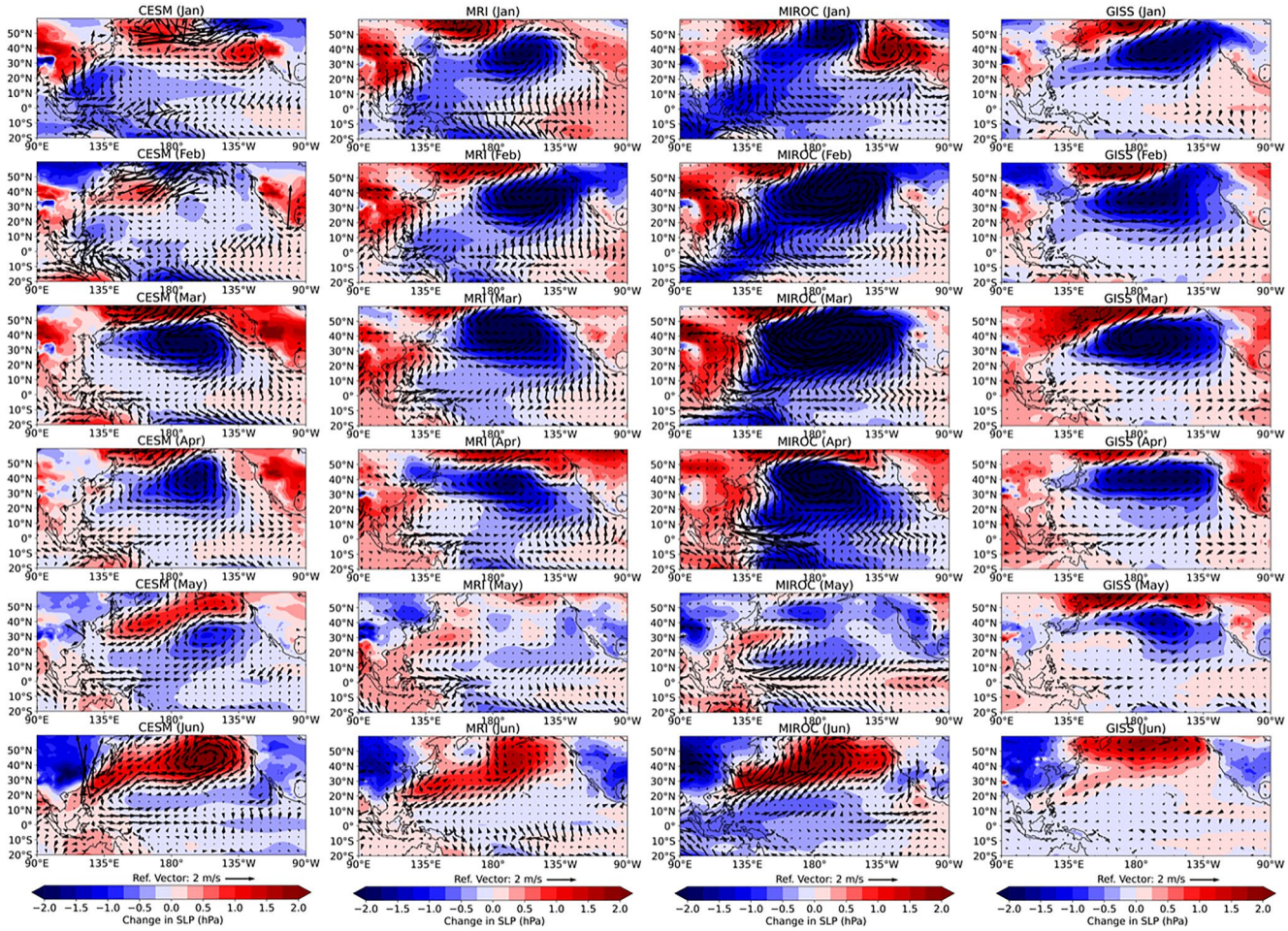

Figure 9. Change in sea level pressure (color shading; units hPa) and near surface winds (vectors) for each model (mid-Holocene minus piControl).

directly associated with the westerly wind anomalies in the western equatorial Pacific through the anomalous low-level wind convergence, consistent with the findings of Erb et al. (2015).

3.3.3. Weakening of the North Pacific Subtropical High

Another mechanism that has been proposed as the source of the westerly wind anomalies in the western Pacific Ocean is a weakening of the North Pacific subtropical anticyclone (Erb et al., 2015). In the control runs of the PMIP4 models, the North Pacific subtropical anticyclone is characterized by a high pressure system in the extratropical Pacific Ocean, centered around 40°N. In the mid-Holocene simulations, a negative sea level pressure anomaly develops over the North Pacific from roughly January to April (typically maximizing in February and March) under reduced insolation in the Northern Hemisphere extratropics and cooling over Asia during the onset of the monsoon season. This weakening of the North Pacific Subtropical High produces a cyclonic wind anomaly that extends into the subtropics, corresponding with the timing of the westerly wind anomalies in the western equatorial Pacific. However, in the western equatorial Pacific, the westerly wind anomalies appear largely decoupled from this circulation feature (Figure 9), and in all models, the weakened subtropical high diminishes in April and disappears by May, when the westerly wind anomalies are well developed in the western Pacific. The onset and demise of the westerly wind anomalies appear more closely tied to the zonal temperature gradient in the Maritime Continent and western Pacific, suggesting that the land-ocean heating contrast in the western Pacific is the dominant source of the westerly wind anomalies. Idealized model simulations would be needed to identify the mechanisms of the low-level wind response in the western Pacific more fully.

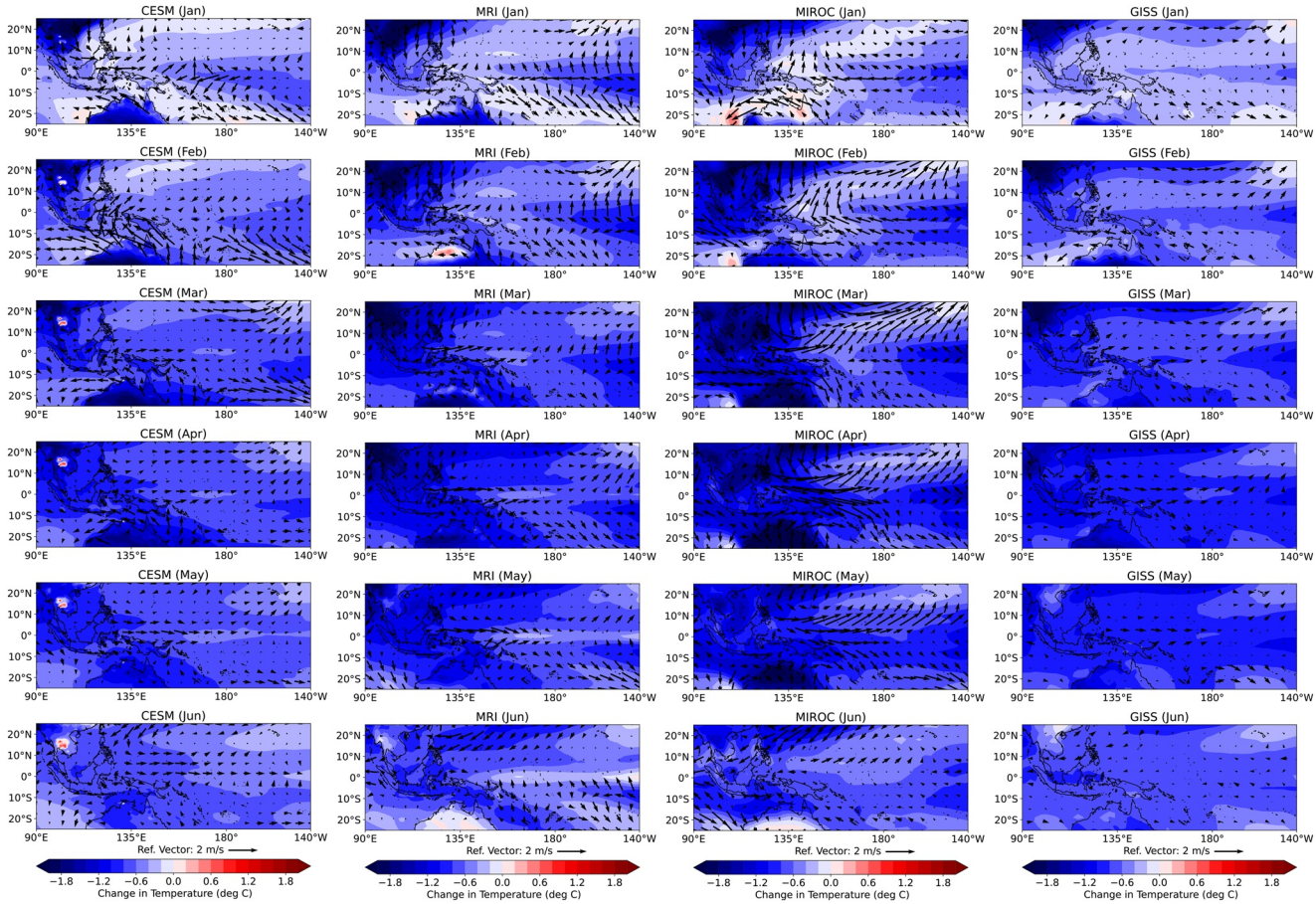

Figure 10. Change in surface air temperature (color shading, unit: °C) and near surface winds (vectors) for each model (mid-Holocene minus piControl).

4. Summary and Conclusion

In this paper, the tropical Pacific annual cycle and ENSO are studied in simulations of the mid-Holocene in four PMIP4/CMIP6 models. Our analysis shows that ENSO variability is modestly reduced during the mid-Holocene, alongside a reduction in the annual cycle of the tropical Pacific cold tongue, consistent with PMIP3 models. These findings indicate that the frequency entrainment mechanism is not the cause of the simulated mid-Holocene ENSO reduction (e.g., Chang et al., 1994; Jin et al., 1994; Tziperman et al., 1994). Furthermore, consistent with the PMIP3 mid-Holocene simulations, the changes in the annual cycle of the Pacific cold tongue are associated with westerly wind anomalies in the western equatorial Pacific in early boreal spring. The westerly wind anomalies are responsible for generating an annual downwelling Kelvin wave that propagates into the central/eastern Pacific in boreal summer (the ENSO growth season), deepening the thermocline. Previous studies have demonstrated that this annual thermocline response weakens the ocean-atmosphere coupling and dampens the growth of ENSO events.

Two mechanisms appear to drive the westerly wind anomalies in the western tropical Pacific. The dominant mechanism involves a shift in convection in the western Pacific driven by a land-ocean heating contrast. More specifically, under reduced insolation, the tropical land regions to the west of the Pacific basin, including the Maritime Continent, cool more the western Pacific Ocean from January to June (most pronounced in March/April), driving westerly wind anomalies and a shift of precipitation from land to ocean in the western Pacific Ocean. The westerly wind anomalies may be further enhanced by a weakening of the North Pacific subtropical anticyclone, though the timing of the westerly wind anomalies appears to be more closely tied to the land-ocean heating contrast.

By probing the mechanisms that lead to reduced ENSO variability and annual cycle of the cold tongue in the mid-Holocene, this work will yield important insights into the response of ENSO to external forcing and linkages between the tropical Pacific annual cycle and ENSO. Since our results are based on four global climate/Earth System models, it is warranted to determine whether these mechanisms are supported by idealized model simulations of the tropical Pacific, in which the dynamical mechanisms of the annual cycle and ENSO responses can be better isolated. Our expectation is that idealized dynamical models will reproduce the annual cycle and ENSO reductions, given the large-scale thermodynamically-driven temperature response in the western tropical Pacific and the robustness of the wind and thermocline responses across a myriad of global climate models with varying representations of tropical Pacific climate.

Other important questions remain for future work. For example, there is a well-known asymmetry between El Niño events and La Niña events (e.g., Clarke & Zhang, 2019) as well as different "flavors" of El Niño events (e.g., Karamperidou et al., 2015). How do different types of events respond to mid-Holocene forcing and are the same set of mechanisms involved in each type of event? These will be interesting topics for future work.

Data Availability Statement

Data sets used in this study can be found at the following websites: CMIP6 PMIP4: https://esgf-node.llnl.gov/search/cmip6/; ERSST V5: https://psl.noaa.gov/data/gridded/data.noaa.ersst.v5.html.

Acknowledgments
We gratefully acknowledge support from the Open Research Program: State Key Laboratory of Tropical Oceanography, South China Sea Institute of Oceanography, Chinese Academy of Sciences Award LT01802, funding from the Japan Society for the Promotion of Science (JSPS) KAKENHI (grant JP19H05703). This material is based upon work supported by the National Science Foundation Paleo Perspective on Climate Change (P2C2) Grant MG&G-1903640 awarded to A. R. A. and K. M. C. Key Laboratory of Physical Oceanography visiting Fellowship Program, Ocean University of China.

References

An, S. I., & Choi, J. (2014). Mid-Holocene tropical Pacific climate state, annual cycle, and ENSO in PMIP2 and PMIP3. *Climate Dynamics*, *43*(3–4), 957–970. https://doi.org/10.1007/s00382-013-1880-z

Baldwin, M. P., Ayarzagüena, B., Birner, T., Butchart, N., Butler, A. H., Charlton-Perez, A. J., et al. (2021). Sudden stratospheric warmings. *Reviews of Geophysics*, *59*(1), e2020RG000708. https://doi.org/10.1029/2020RG000708

Battisti, D. S., & Hirst, A. C. (1989). Interannual variability in a tropical atmosphere–ocean model: Influence of the basic state, ocean geometry and nonlineary. *Journal of the Atmospheric Sciences*, *46*(12), 1687–1712. https://doi.org/10.1175/1520-0469(1989)046<1687:iviata>2.0.co;2

Brown, J. R., Brierley, C. M., An, S.-I., Guarino, M.-V., Stevenson, S., Williams, C. J. R., et al. (2020). Comparison of past and future simulations of ENSO in CMIP5/PMIP3 and CMIP6/PMIP4 models. *Climate of the Past*, *16*(5), 1777–1805. https://doi.org/10.5194/cp-16-1777-2020

Carré, M., Braconnot, P., Elliot, M., d'Agostino, R., Schurer, A., Shi, X., et al. (2021). High-resolution marine data and transient simulations support orbital forcing of ENSO amplitude since the mid-Holocene. *Quaternary Science Reviews*, *268*, 107125. https://doi.org/10.1016/j.quascirev.2021.107125

Chang, C.-P., Wang, Z., McBride, J., & Liu, C.-H. (2005). Annual cycle of Southeast Asia–Maritime Continent rainfall and the asymmetric monsoon transition. *Journal of Climate*, *18*(2), 287–301. https://doi.org/10.1175/JCLI-3257.1

Chang, P., Wang, B., Li, T., & Ji, L. (1994). Interactions between the seasonal cycle and the Southern Oscillation-Frequency entrainment and chaos in a coupled ocean-atmosphere model. *Geophysical Research Letters*, *21*(25), 2817–2820. https://doi.org/10.1029/94gl02759

Chiang, J. C. H., Fang, Y., & Chang, P. (2009). Pacific climate change and ENSO activity in the mid-Holocene. *Journal of Climate*, *22*(4), 923–939. https://doi.org/10.1175/2008jcli2644.1x

Clarke, A. J., & Zhang, X. (2019). On the physics of the El Niño/warm water volume phase diagram. *Journal of Physical Oceanography*, *49*(6), 1541–1560. https://doi.org/10.1175/jpo-d-18-0144.1

Clarke, J. A. (2014). El Niño physics and El Niño predictability. *Annual Review of Marine Science*, *6*(1), 79–99. https://doi.org/10.1146/annurev-marine-010213-135026

Clement, A. C., Seager, R., & Cane, M. A. (1999). Orbital controls on the El Niño/Southern Oscillation and the tropical climate. *Paleoceanography*, *14*(4), 441–456. https://doi.org/10.1029/1999PA900013

Cobb, K. M., Westphal, N., Sayani, H. R., Watson, J. T., Lorenzo, E. D., Cheng, H., et al. (2013). Highly variable El Niño–Southern Oscillation throughout the Holocene. *Science*, *339*(6115), 67–70. https://doi.org/10.1126/science.1228246

Danabasoglu, G., Lamarque, J.-F., Bacmeister, J., Bailey, D. A., DuVivier, A. K., Edwards, J., et al. (2019). The Community Earth System Model Version 2 (CESM2). *Journal of Advances in Modeling Earth Systems*, *12*, e2019MS001916. https://doi.org/10.1029/2019MS001916

Emile-Geay, J., Cobb, K. M., Carré, M., Braconnot, P., Leloup, J., Zhou, Y., et al. (2016). Links between tropical Pacific seasonal, interannual and orbital variability during the Holocene. *Nature Geoscience*, *9*(2), 168–173. https://doi.org/10.1038/ngeo2608

Erb, M. P., Broccoli, A. J., Graham, N. T., Clement, A. C., Wittenberg, A. T., & Vecchi, G. A. (2015). Response of the equatorial pacific seasonal cycle to orbital forcing. *Journal of Climate*, *28*(23), 9258–9276. https://doi.org/10.1175/jcli-d-15-0242.1

Hajima, T., Watanabe, M., Yamamoto, A., Tatebe, H., Noguchi, M. A., Abe, M., et al. (2020). Development of the MIROC-ES2L Earth system model and the evaluation of biogeochemical processes and feedbacks. *Geoscientific Model Development*, *13*(5), 2197–2244. https://doi.org/10.5194/gmd-13-2197-2020

Harrison, D., & Vecchi, G. (1999). On the termination of El Niño. *Geophysical Research Letters*, *26*(11), 1593–1596. https://doi.org/10.1029/1999gl900316

Jin, F.-F., Neelin, J., & Ghil, M. (1994). El Niño on the devil's staircase: Annual and subharmonic steps to chaos. *Science*, *264*(5155), 70–72. https://doi.org/10.1126/science.264.5155.70

Jin, F.-F., Neelin, J., & Ghil, M. (1996). El Niño/Southern Oscillation and the annual cycle: Subharmonic frequency-locking and aperiodicity. *Physica D*, *98*(2–4), 442–465. https://doi.org/10.1016/0167-2789(96)00111-x

Karamperidou, C., Di Nezio, P. N., Timmermann, A., Jin, F. F., & Cobb, K. M. (2015). The response of ENSO flavors to mid-Holocene climate: Implications for proxy interpretation. *Paleoceanography*, *30*(5), 527–547. https://doi.org/10.1002/2014pa002742

Kelley, M., Schmidt, G. A., Nazarenko, L., Bauer, S. E., Ruedy, R., Russell, G. L., et al. (2020). GISS-E2.1: Configurations and climatology. *Journal of Advances in Modeling Earth Systems*, *12*(8), e2019MS002025. https://doi.org/10.1029/2019MS002025

Koutavas, A., & Joanides, S. (2012). El Niño-Southern Oscillation extrema in the Holocene and last glacial maximum. *Paleoceanography*, *27*(4), PA4208. https://doi.org/10.1029/2012PA002378

Liu, Z. (2002). A simple model study of ENSO suppression by external periodic forcing. *Journal of Climate*, *15*(9), 1088–1098. https://doi.org/10.1175/1520-0442(2002)015<1088:asmsoe>2.0.co;2

Liu, Z., Kutzbach, J., & Wu, L. (2000). Modeling climate shift of El Niño variability in the Holocene. *Geophysical Research Letters*, *27*(15), 2265–2268. https://doi.org/10.1029/2000gl011452

Liu, Z., Lu, Z., Wen, X., Otto-Bliesner, B., Timmermann, A., & Cobb, K. (2014). Evolution and forcing mechanisms of El Niño over the past 21,000 years. *Nature*, *515*(7528), 550–553. https://doi.org/10.1038/nature13963

McGregor, H., Fischer, M., Gagan, M., Fink, D., Phipps, S. J., Wong, H., & Woodroffe, C. D. (2013). A weak El Niño/Southern Oscillation with delayed seasonal growth around 4,300 years ago. *Nature Geoscience*, *6*(11), 949–953. https://doi.org/10.1038/ngeo1936

McGregor, S., Timmermann, A., Schneider, N., Stuecker, M., & England, M. H. (2012). The effect of the south Pacific convergence zone on the termination of El Niño events and the meridional asymmetry of ENSO. *Journal of Climate*, *25*(16), 5566–5586. https://doi.org/10.1175/jcli-d-11-00332.1

Otto-Bliesner, B. L., Braconnot, P., Harrison, S. P., Lunt, D. J., Abe-Ouchi, A., Albani, S., et al. (2017). The PMIP4 contribution to CMIP6—Part 2: Two interglacials, scientific objective and experimental design for Holocene and Last Interglacial simulations. *Geoscientific Model Development*, *10*(11), 3979–4003. https://doi.org/10.5194/gmd-10-3979-2017

Pan, A., Liu, Q., & Liu, Z. (2005). Periodic forcing and ENSO suppression in the Cane-Zebiak model. *Journal of Oceanography*, *61*(1), 109–113. https://doi.org/10.1007/s10872-005-0023-5

Roberts, W. H. G., Battisti, D., Hartmann, D., & Bretherton, C., (2007). *An investigation into the causes for the reduction in the variability of the El Niño-Southern Oscillation in the early Holocene in a global climate model (PhD thesis)*. University of Washington.

Schneider, T., Bischoff, T., & Haug, G. H. (2014). Migrations and dynamics of the intertropical convergence zone. *Nature*, *513*(7516), 45–53. https://doi.org/10.1038/nature13636

Song, M.-E., & Chen, L. (2022). Responses of tropical background state and ENSO behaviors to mid-Holocene forcing simulated by PMIP3 and PMIP4 models. *Frontiers of Earth Science*, *10*, 853577. https://doi.org/10.3389/feart.2022.853577

Stein, K., Timmermann, A., & Schneider, N. (2011). Phase synchronization of the El Niño-Southern Oscillation with the annual cycle. *Physical Review Letters*, *107*(12), 128501. https://doi.org/10.1103/physrevlett.107.128501

Tziperman, E., Cane, M., & Zebiak, S. (1995). Irregularity and locking to the seasonal cycle in an ENSO prediction model as explained by the quasi-periodicity route to chaos. *Journal of the Atmospheric Sciences*, *52*(3), 293–306. https://doi.org/10.1175/1520-0469(1995)052<0293:ialtts>2.0.co;2

Tziperman, E., Stone, L., Cane, M. A., & Jarosh, H. (1994). El Niño chaos: Overlapping of resonances between the seasonal cycle and the Pacific Ocean-atmosphere oscillator. *Science*, *264*(5155), 72–74. https://doi.org/10.1126/science.264.5155.72

Walker, G. T. (1924). Correlation in seasonal variations of weather. IX. A further study of world weather. *Memoirs of the India Meteorological Department*, *24*(9), 275–332. https://doi.org/10.1002/qj.49705021136

Wang, B., & Fang, Z. (1996). Chaotic oscillation of the tropical climate: A dynamic system theory for ENSO. *Journal of the Atmospheric Sciences*, *53*(19), 2786–2802. https://doi.org/10.1175/1520-0469(1996)053<2786:cootca>2.0.co;2

Yukimoto, S., Kawai, H., Koshiro, T., Oshima, N., Yoshida, K., Urakawa, S. S., et al. (2019). The meteorological Research Institute Earth system model version 2.0, MRI-ESM2.0: Description and basic evaluation of the physical component. *Journal of the Meteorological Society of Japan*, *97*(5), 931–965. https://doi.org/10.2151/jmsj.2019-051

Zebiak, S. E., & Cane, M. A. (1987). A model El Niño and Southern Oscillation. *Monthly Weather Review*, *115*(10), 2262–2278. https://doi.org/10.1175/1520-0493(1987)115<2262:ameno>2.0.co;2

Erratum

In the originally published version of this article, Figures 8 and 10 had incorrect wind vectors. Also, the caption for Figure 5 was missing the model number. These matter have since been corrected and this version may be considered the authoritative version of record.